Hair cell α9α10 nicotinic acetylcholine receptor functional expression regulated by ligand binding and deafness gene products

Shenyan Gu[a,1], Daniel Knowland[a,1], Jose A. Matta[a,1], Min L. O'Carroll[a,1], Weston B. Davini[a,1], Madhurima Dhara[a], Hae-Jin Kweon[a], and David S. Bredt[a,2]

[a]Neuroscience Discovery, Janssen Pharmaceutical Companies of Johnson & Johnson, San Diego, CA 92121

Edited by Roger A. Nicoll, University of California, San Francisco, CA, and approved August 18, 2020 (received for review July 1, 2020)

Auditory hair cells receive olivocochlear efferent innervation, which refines tonotopic mapping, improves sound discrimination, and mitigates acoustic trauma. The olivocochlear synapse involves α9α10 nicotinic acetylcholine receptors (nAChRs), which assemble in hair cells only coincident with cholinergic innervation and do not express in recombinant mammalian cell lines. Here, genome-wide screening determined that assembly and surface expression of α9α10 require ligand binding. Ion channel function additionally demands an auxiliary subunit, which can be transmembrane inner ear (TMIE) or TMEM132e. Both of these single-pass transmembrane proteins are enriched in hair cells and underlie nonsyndromic human deafness. Inner hair cells from TMIE mutant mice show altered postsynaptic α9α10 function and retain α9α10-mediated transmission beyond the second postnatal week associated with abnormally persistent cholinergic innervation. Collectively, this study provides a mechanism to link cholinergic input with α9α10 assembly, identifies unexpected functions for human deafness genes TMIE/TMEM132e, and enables drug discovery for this elusive nAChR implicated in prevalent auditory disorders.

nAChR | α9α10 | TMIE | tinnitus | cochlea

Cochlear hair cells are unique among our primary sensory cells in that they receive efferent innervation from the brain (1). This input, originating from medial olivocochlear neurons, is activated by sound and provides negative feedback (2, 3). In the canonical pathway, acetylcholine (ACh) released from medial olivocochlear terminals activates a nicotinic ACh receptor (nAChR) on outer hair cells (OHC) that tightly couples to a calcium-activated, small conductance SK2 potassium channel that suppresses OHC electromotility (4, 5). This olivocochlear network improves signal discrimination amid background noise, protects against sound-induced hearing loss, and modulates synapse formation (2, 3). Accordingly, this pathway provides compelling pharmacological targets for acoustic trauma, presbycusis, and tinnitus.

Therapeutically most attractive in this pathway is the α9α10 nAChR, which has unique pharmacology and a selective distribution on cochlear and vestibular hair cells (6, 7). Nicotinic AChRs comprise a large family of pentameric ion channels formed from nine α (α2 to α10) and three β (β2 to β4) subunits. These receptors are broadly expressed in brain and periphery and mediate physiological effects of ACh as well as addictive properties of nicotine (8–14). The heteromeric nAChR on hair cells contains α9 and α10 subunits and has several distinguishing characteristics (15, 16). The α9α10 receptor features antagonism by nicotine, which typically agonizes nAChRs, and potent block by strychnine and bicuculline, which typically antagonize glycine and GABA receptors, respectively (15, 16). The α9α10 nAChR is among the most calcium-selective ligand-gated channels known (17), and its endogenous activity has only been recorded in cochlear and vestibular hair cells.

Studies of α9 and α10 mutant mice have provided keen insights regarding physiological roles for the medial olivocochlear pathway (2, 3). Targeted disruption of either α9 (18) or α10 (19) abolishes ACh-mediated synaptic currents in both inner and outer hair cells. Whereas these knockout mice show normal tone detection and sound-intensity discrimination, they display several auditory processing deficits, including abnormal sound localization (20) and impaired selective attention (21). Mice lacking α9 also have abnormalities in cochlear as well as central auditory synapse formation, and in tonotopic map refinement (22, 23). Conversely, gain-of-function mutation of α9 protects mice from acoustic synaptopathy (24). As both hypo- and hyperfunction of the cholinergic efferent synapse have profound auditory effects, elucidating molecular mechanisms that control α9α10 receptor function has important scientific and medical implications.

Understanding of α9α10 physiology has been hampered because this receptor does not functionally express in recombinant cell lines (15, 25). Whereas injection of α9 and α10 complementary RNAs into oocytes reconstitutes α9α10 receptors, transfection of α9 and α10 into mammalian cells does not yield ACh binding sites or ACh-gated channels (25). Assembly of α9α10 channels in cochlear hair cells also displays fascinating peculiarities. Developmental studies

Significance

Auditory hair cells receive olivocochlear efferent innervation, which improves sound discrimination and mitigates acoustic trauma. The olivocochlear synapse involves α9α10 nicotinic acetylcholine receptors (nAChRs), which do not express in recombinant cell lines. Here, genome-wide screening determined that assembly and surface expression of α9α10 require ligand binding. Ion channel function additionally demands an auxiliary subunit, which can be transmembrane inner ear (TMIE) or TMEM132e. These single-pass transmembrane proteins are enriched in hair cells and underlie nonsyndromic human deafness. Inner hair cells from TMIE mutant mice show altered postsynaptic α9α10 function and abnormally retain α9α10-mediated transmission through development. This study identifies unexpected functions for human deafness genes TMIE/TMEM132e and enables drug discovery for this elusive nAChR implicated in prevalent auditory disorders.

Author contributions: S.G., D.K., J.A.M., M.L.O., W.B.D., and D.S.B. designed research; D.S.B. supervised the project; S.G., D.K., J.A.M., M.L.O., W.B.D., M.D., and H.-J.K. performed research; S.G., D.K., J.A.M., M.L.O., W.B.D., M.D., and H.-J.K. analyzed data; and S.G., D.K., J.A.M., and D.S.B. wrote the paper.

Competing interest statement: All of the authors are all full-time employees of Janssen Pharmaceutical Companies of Johnson & Johnson. The authors declare a patent application on reconstitution of α9α10 receptors using choline acetyltransferase and either TMIE or TMEM132 family proteins, which was filed in the United States (PCT# 62/849,653).

This article is a PNAS Direct Submission.

[1]S.G., D.K., J.A.M., M.L.O., and W.B.D. contributed equally to this work.

[2]To whom correspondence may be addressed. Email: DBredt@its.jnj.com.

This article contains supporting information online at https://www.pnas.org/lookup/suppl/doi:10.1073/pnas.2013762117/-/DCSupplemental.

First published September 14, 2020.

show that functional α9α10 receptors and the mRNA for α10 occur transiently in inner hair cells (IHCs) prior to the onset of hearing around postnatal day 12 (P12) (26). In contrast, OHC α9α10 receptor function appears only after hearing onset and persists through adulthood (2). These dynamics of postsynaptic α9α10 function closely match the timing of presynaptic cholinergic innervations on IHCs and OHCs (27), which may imply a functional link. Molecular mechanisms that determine these features of α9α10 functional expression in hair cells are unknown. Whereas NACHO protein is essential for α7 nAChRs (28), accessory proteins that enable assembly and function of α9α10 receptors have remained mysterious.

Here, we used genome-wide complementary DNA (cDNA) screening to identify functional partners for α9α10. Remarkably, we found that α9α10 channels can be reconstituted by coexpression of either transmembrane inner ear (TMIE) or TMEM132e, two unrelated products of human deafness genes expressed in hair cells (29, 30). Both TMIE and TMEM132e are implicated in mechanotransduction (MET) near the tips of hair cell stereocilia, but their presence at the base of hair cells (30, 31) suggests they also have other unknown roles. TMIE expression is a necessary component of the hair cell MET channel (31), and we find that TMIE additionally serves as an α9α10 auxiliary subunit. Our cDNA screening also found that choline acetyltransferase (ChAT), the biosynthetic enzyme for ACh, synergizes with TMIE or TMEM132e to enable α9α10 receptor function. This synergy reflects the fact that functional α9α10 expression strictly requires ligand-binding, which can be provided by extracellular application of ACh or the membrane impermeable polypeptide antagonist α-bungarotoxin (α-Bgt). IHCs from TMIE mutant mice show up-regulation of neonatal α9α10 channel function as well as abnormal persistence of cholinergic innervation and α9α10 synaptic transmission beyond P12. These studies identify unexpected functions for deafness gene products TMIE and TMEM132e in controlling α9α10 nAChRs, provide a mechanism to couple cholinergic innervation to postsynaptic nAChR expression, and enable drug discovery for auditory disorders associated with these hair cell receptors.

Results

Genomic cDNA Screening Identifies Factors That Enable α9α10 Receptor Reconstitution. To search for gene products that can enable heterologous α9α10 receptor reconstitution, we first designed a library of 3,025 cDNAs that encode proteins whose mRNAs are enriched in the brain (see *Methods* for algorithm). We next cotransfected α9- and α10-encoding plasmids along with individual clones from this cDNA library into human embryonic kidney (HEK293T) cells grown in 384-well plates. Two days after transfection, cells were stimulated with ACh (250 μM) in the presence of scopolamine (50 nM), and intracellular Ca^{2+} was detected with a FLIPR (fluorescent imaging plate reader) instrument. As previously published (15, 25), α9α10-transfected HEK cells lacked ACh-evoked responses. High-throughput cDNA screening identified significant Ca^{2+} signals in three distinct wells, which contained plasmids encoding TMIE, ChAT, or TMEM132d (*SI Appendix*, Table S1). Because TMEM132d was not previously detected in the inner ear (32), we initially focused on TMIE and ChAT, which are enriched in cochlear hair cells (33) and hair cell-innervating nerve terminals (34), respectively. Follow-up Ca^{2+} fluorescence experiments showed that cotransfection of α9α10 with either TMIE or ChAT enabled sustained ACh-evoked responses from α9α10 and that TMIE and ChAT together showed powerful synergy on α9α10 (Fig. 1 *A* and *B*). The pharmacology of these α9α10 receptors resembled the unique features of the cholinergic synapse at cochlear hair cells, such that ACh, carbachol, and dimethylphenylpiperazinium (DMPP) were agonists whereas nicotine, atropine, strychnine, and methyllycaconitine (MLA) were antagonists (Fig. 1 *C* and *D*). In contrast, ChAT and TMIE plasmids had no significant effect on nAChR α7, 5-HT3A serotonin, or GluA1 glutamate receptors (Fig. 1*B*).

We were struck that α9α10 functional expression was specifically enabled by ChAT, the biosynthetic enzyme for ACh, and by TMIE, a deafness gene product (29) enriched in cochlear hair cells (33). TMIE has been characterized as a two-pass transmembrane (TM) protein that associates with the MET channel subunits TMC1/2 (35) such that the N-terminal TM domain of TMIE was purported to regulate MET gating, whereas the C-terminal part of TMIE is critical for binding TMC1/2 and for channel function (31). A single TMIE gene is present in species as primitive as *Drosophila*, whose ortholog (DTMIE) has only one TM domain (*SI Appendix*, Fig. S1*A*). Importantly, we found that DTMIE reconstituted human α9α10 function and that DTMIE synergized with ChAT on human α9α10 (Fig. 1*B*). We therefore inferred that the first hydrophobic helix in mammalian TMIE may be a signal sequence, which conflicts with a recent publication (31).

Supporting our hypothesis, we achieved full functional α9α10 reconstitution using a TMIE construct (SP-TMIE) that replaced its first hydrophobic helix with the signal peptide from GluA1 (*SI Appendix*, Fig. S1 *B* and *D*). To assess TMIE processing directly, we also constructed a version (N-HA TMIE) with an N-terminal HA-tag (*SI Appendix*, Fig. S1*E*). Immunoblotting of transfected cell lysates showed that the N-terminal tag on TMIE was quantitatively removed as expected with cleavage of a signal peptide (lane 3 in *SI Appendix*, Fig. S1 *F* and *G*). Furthermore, proteins from SP-TMIE and N-HA TMIE showed the same apparent molecular weight as did wild-type TMIE, whereas a version with an HA-tag in the cytoplasmic region (C-HA TMIE) showed a slightly slower migration on SDS/PAGE (*SI Appendix*, Fig. S1*G*). These data conclusively demonstrate that mammalian and *Drosophila* TMIEs are single-pass TM proteins whose actions on α9α10 are phylogenetically conserved.

To assess effects of ChAT and TMIE on α9α10 ion channel function, we performed electrophysiological studies. As previously published (25), patch-clamp studies showed no response to ACh in HEKs transfected with α9 and α10. Cotransfection with TMIE but not ChAT produced small ACh-evoked responses. Remarkably, cotransfection with TMIE + ChAT reconstituted large ACh-evoked desensitizing responses (Fig. 1 *E* and *F*) that have never before been detected from α9α10 in cell transfections.

In nonnative cell types, most nAChRs, including α9α10, do not efficiently assemble as pentamers and do not properly traffic to the cell surface (25). To investigate effects of TMIE and ChAT on α9α10 surface expression, we added an HA-tag to the extracellular C terminus of α9. Such tagging does not affect α9α10 channel function (*SI Appendix*, Fig. S1 *C* and *D*) and enables surface nAChR quantification by immunolabeling nonpermeabilized cells (28). In cells transfected with α9α10 alone, there was no detectable surface labeling, and this was not affected by TMIE. Strikingly, ChAT cotransfection produced clear surface α9α10 immunofluorescence that was not augmented by adding TMIE (Fig. 2 *A* and *B*). ChAT but not TMIE also enhanced α4β2 surface expression (*SI Appendix*, Fig. S2). On the other hand, neither TMIE nor ChAT significantly affected α7 or 5-HT3A (Fig. 2 *A* and *B* and *SI Appendix*, Fig. S2).

We next assessed whether TMIE or ChAT influence α9α10 assembly, which can be probed with an orthosteric ligand, such as [^{3}H]MLA, which only binds at the interface between folded subunits. Consistent with previous studies (25), [^{3}H]MLA binding was undetectable in cells transfected with α9 + α10, and TMIE did not affect this. In contrast, ChAT dramatically increased [^{3}H]MLA binding, and TMIE failed to enhance this further (Fig. 2*C*).

These data show that ChAT enables α9α10 assembly and surface expression and is prerequisite for robust functional enhancement of channel activity by TMIE. We wondered if additional α9α10-enhancing proteins might be identified by cotransfection with ChAT. We therefore performed genome-wide screening of 21,968 cDNA

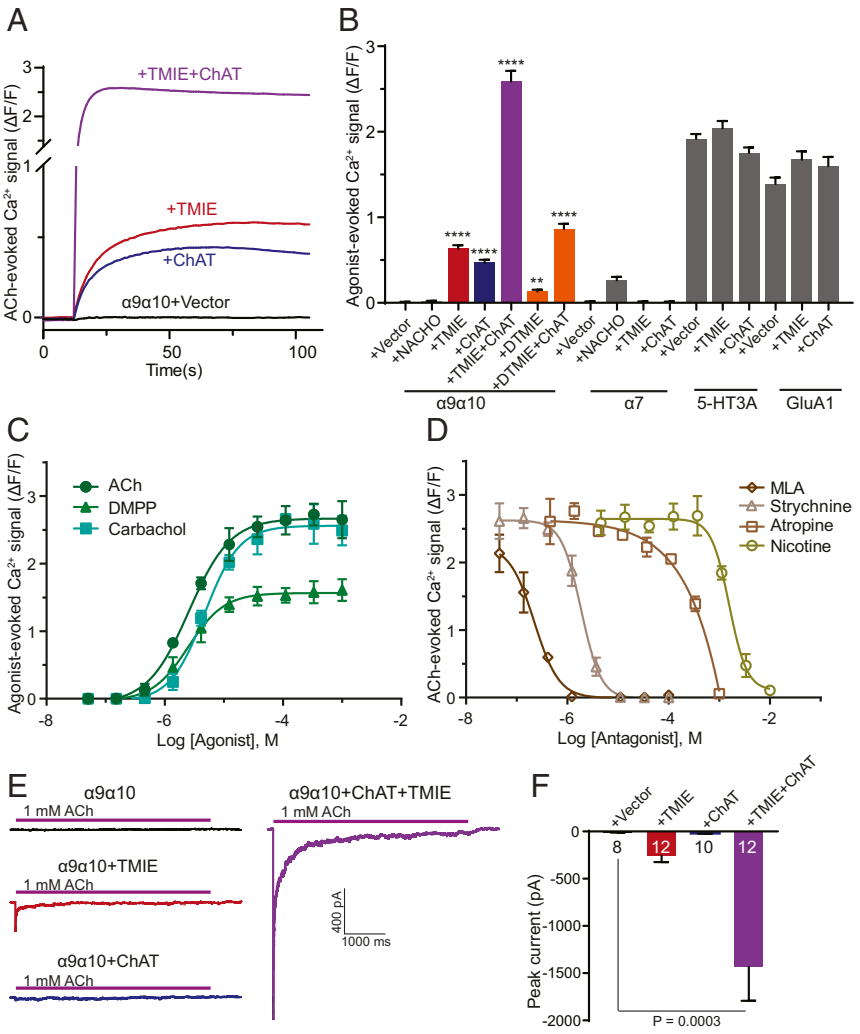

Fig. 1. ChAT and TMIE conspire for α9α10 receptor reconstitution. (*A*) FLIPR traces from HEK cells transfected as indicated and stimulated with 250 μM ACh. (*B*) Quantification of FLIPR responses from HEK cells transfected as indicated and stimulated with 250 μM ACh for α9α10, α7, 100 μM serotonin for 5-HT3A and 100 μM glutamate + 100 μM cyclothiazide (CTZ) for GluA1. (DTMIE: *Drosophila* TMIE). Data shown are from a representative experiment (mean ± SD, $n = 8$, $^{**}P \leq 0.01$, $^{****}P \leq 0.0001$, for comparison to α9α10 control, one-way ANOVA, Dunnett's test) that was replicated with similar results. (*C* and *D*) Pharmacological characterization of α9α10 receptor reconstituted in HEK cells. Agonist and antagonist concentration-response curves from HEK 293T cells transfected with plasmids encoding α9α10 + ChAT + TMIE (mean ± SD, $n = 3$). ACh EC_{50} = 2.6 μM; carbachol EC_{50} = 4.7 μM; DMPP EC_{50} = 2.5 μM. Antagonist experiments used 25 μM ACh: nicotine IC50 = 1,560 μM, atropine IC50 = 400 μM, strychnine IC50 = 1.9 μM, MLA IC50 = 0.22 μM. (*E*) Whole-cell recordings from HEK cells cotransfected with GFP and other plasmids as indicated. Currents from GFP^+ cells were evoked with 1 mM ACh. (*F*) Summary graph of peak currents from *E* (mean ± SEM; *n* as indicated, one-way ANOVA, Tukey's test).

clones [including Origene (28) and Broad Institute (36) cDNA libraries] in cells transfected with α9α10 and ChAT. These studies identified five additional clones encoding proteins—TMEM132a, TMEM132c, TMEM132e, TMEM100, and TNFRSF10a—that synergize with ChAT to enhance α9α10 channel function (*SI Appendix*, Fig. S3*A* and Table S1). In situ hybridization (RNAscope) experiments revealed abundant amounts of TMIE and lesser amounts of TMEM132a and TMEM132e mRNA in cochlear hair cells, which also express functional α9α10 receptors (*SI Appendix*, Fig. S3*B*); therefore, along with ChAT, we prioritized study of TMIE.

Efficient Surface Expression of α9α10 Requires Ligand Binding. Orthosteric ligands typically enhance surface expression of nAChR through a chemical chaperone mechanism (37), which could explain how ChAT promotes α9α10 channel activity and surface expression. To determine whether ACh mediates the effect of ChAT, we cotransfected α9α10 + TMIE + ChAT with acetylcholinesterase (AChE). Indeed, AChE eliminated α9α10 channel activity function in the presence of TMIE and ChAT (Fig. 3 *A* and *B*). Cotransfection with AChE also partially reduced agonist-evoked activity from α4β2 and to lesser extent α7 receptors that were coexpressed with NACHO (Fig. 3*B*). In contrast, AChE did not affect function of GluA1 (Fig. 3*B*). We next assessed effects of AChE on receptor surface expression. We found that cotransfection of AChE almost abolished surface expression of α9α10 and modestly reduced the surface expression of α4β2 and α7 (Fig. 3 *C* and *D*). In contrast, AChE did not affect surface expression of GluA1 (Fig. 3 *C* and *D*). These data suggest that in comparison with other nAChRs, α9α10 receptors strictly relied on ligand binding for functional surface expression.

To explore this ligand-binding requirement, we mutated a critical tryptophan (W176) in the ligand-binding domain of α9 and the analogous residues (W182) in α4 and (W171) in α7. By disrupting ligand binding, this mutation abolished surface expression of α9α10 in the presence of ChAT (Fig. 3 *C* and *D*). In

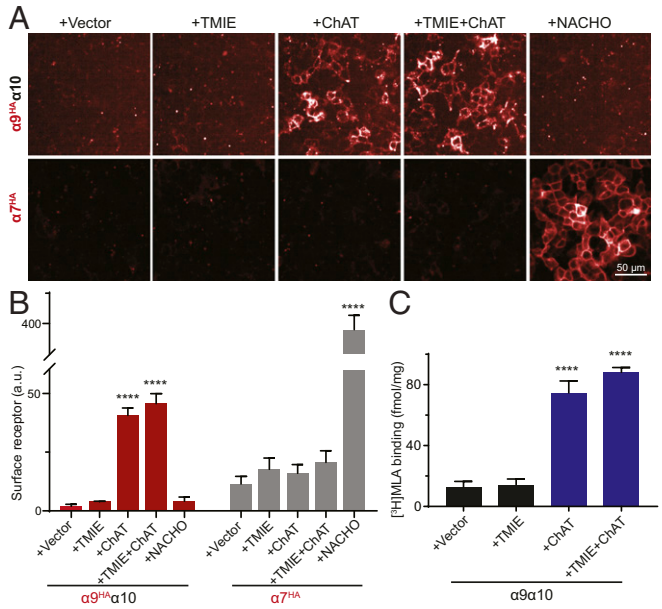

Fig. 2. ChAT promotes α9α10 surface expression and assembly. (*A*) Images of receptor surface expression in non-permeabilized HEK cells transfected with $\alpha9^{HA}$+α10 or $\alpha7^{HA}$ together with other plasmids as indicated. (*B*) Summary graph of receptor surface expression from *A* (mean ± SD, $n = 3$, $^{****}P \leq 0.0001$, for comparison to $\alpha9^{HA}$α10 control, one-way ANOVA, Dunnett's test). (*C*) Specific [^{3}H]MLA (10 nM) binding to HEK cells cotransfected with α9α10 and other plasmids as indicated. Nonspecific binding was not displaced by 100 μM unlabeled MLA. Data are from a representative experiment (mean ± SD, $n = 4$, $^{****}P \leq 0.0001$, for comparison to α9α10 control, one-way ANOVA, Dunnett's test) that was replicated with similar results.

contrast, α4β2 and α7 receptors retained significant surface expression despite the loss of ligand binding (Fig. 3 *C* and *D*). To assess more directly effects of ligand binding on functional assembly of α9α10 receptors, we preincubated transfected cells with ACh or the orthosteric antagonist MLA. For this, we treated α9α10 or α9α10 + TMIE-transfected cells overnight with ACh or MLA and then measured receptor surface expression and ACh-evoked Ca^{2+}signaling. As shown in Figs. 3 *E* and *F* and 4*B*, these agents robustly enabled α9α10 surface expression and channel function. The chemical chaperone effects on α9α10 were impressively large in magnitude and occurred with incubations as short as 1 h (Fig. 3*G*).

ACh-Mediated Enhancement of Assembled α9α10 Receptors Can Occur at the Cell Surface. Nicotinic ligands are proposed to function as chemical chaperones in the biosynthetic pathway (37). However, ACh does not permeate the plasma membrane (38), which seemed inconsistent with effects of ACh incubation on α9α10 assembly. We therefore wondered whether ligand-mediated α9α10 stabilization might occur, in part, on the cell surface. To address this, we developed a chimeric receptor strategy using the TM3/TM4 intracellular loop from α6, which impedes its surface expression (39). As a control, we swapped this loop into α7 and found it blocks surface trafficking of an α7/α6 chimera (*SI Appendix*, Fig. S4 *A*–*C*). We then constructed an analogous α9/α6 chimera (Fig. 4*A*). When cotransfected with ChAT and α10, the α9/α6 chimera did not traffic to the cell surface (Fig. 4*B*). Permeabilized staining showed that total expression levels of the α9 wild-type and α9/α6 were comparable (*SI Appendix*, Fig. S4*E*). We used [^{3}H]MLA binding to assess receptor assembly. Both α9 wild-type and α9/α6 loop chimera showed enhanced assembly when cotransfected with ChAT or when preincubated with MLA (Fig. 4*C*), which permeates cell membranes (40). Importantly however, preincubation with ACh only enhanced levels of assembled wild-type α9 but not the α9/α6 loop chimera (Fig. 4*C*). This confirms that ACh was not permeating the cell membrane yet was stabilizing assembled α9α10 receptors on the cell surface. To address this further, we preincubated cells with α-Bgt, a large cell-impermeant toxin antagonist of certain nAChRs, including α9α10 (15). Strikingly, preincubation with α-Bgt conferred robust α9α10 function (Fig. 4*D*), indicating that ligand-mediated α9α10 stabilization can occur at the cell surface.

TMIE Promotes α9α10 Function by Acting as an Auxiliary Subunit. Because TMIE had no effect on α9α10 receptor assembly or trafficking, we explored TMIE effects on channel gating. To enhance functional expression of α9α10 receptors for electrophysiological recordings, transfected cells were preincubated with ACh for 24 h. These patch-clamp studies showed that α9α10 channels display similar rates of desensitization when cotransfected with either ChAT or TMIE (Fig. 5 *A* and *B*). On the other hand, TMIE significantly slowed α9α10 deactivation as compared to channels cotransfected with ChAT (Fig. 5 *C* and *D*). This effect on channel gating implies direct interaction of TMIE with the α9α10 receptor. TMIE has also been reported as a component of the hair cell MET channel (31). Furthermore, a point mutation in TMIE, Arg92Trp (R92W) that causes human deafness, cannot support MET function in hair cells (35) and is essential for phosphatidylinositol bisphosphate binding to TMIE (31). Whereas the rat R92W mutation blocks surface expression of rat TMIE (35), this mutation does not impair surface expression of human TMIE (Fig. 5*E* and *SI Appendix*, Fig. S5*A*). Importantly, the R92W mutation nearly abolished TMIE reconstitution of α9α10 channel function without affecting receptor surface expression (Fig. 5 *E* and *F* and *SI Appendix*, Fig. S5 *A* and *B*).

These functional data suggest that TMIE associates with α9α10 on the cell surface. To assess physical interaction, we performed coimmunoprecipitation experiments from cRNA-injected oocytes, which provide a robust assay system for validation of receptor-associated subunits (41). Following cRNA injection, solubilized oocyte membrane proteins were immunoprecipitated with TMIE antibody and analyzed by immunoblotting. These experiments showed that α9α10 specifically and efficiently coimmunoprecipitated with TMIE, whereas 5-HT3A and GluA1 did not, confirming stable interaction of α9α10 and TMIE (Fig. 5*G* and *SI Appendix*, Fig. S5*C*).

α9α10 Function Is Markedly Enhanced in TMIE Mutant Mice. To assess the effect of TMIE on α9α10 function in vivo, we recorded hair cell activity in *Spinner* $TMIE^{sr\text{-}2J}$ mice. This line (TMIE mutant) has a point mutation in the exon five splice acceptor site, which is predicted to disrupt the protein's TM domain. To assess mutant TMIE transcripts in *Spinner*, we performed RT-PCR and sequencing (*SI Appendix*, Fig. S6*A*). As expected, the *Spinner* mutation perturbed exon 4/5 splicing and yielded an array of aberrant TMIE transcripts, all of which were null for α9α10 functional expression (*SI Appendix*, Fig. S6*B*).

Next, we performed whole-cell recordings on IHCs in acutely isolated apical turns of the cochlear organ from wild-type and TMIE mutant mice. Previous studies found that prior to hearing onset (<P12), application of high concentration of KCl induces synaptic events involving calcium influx through IHC α9α10 receptors that tightly couples to the calcium-sensitive potassium channel SK2 (42). Indeed, superfusion of 40 mM KCl reliably induced synaptic events superimposed on a steady inward depolarizing current in IHCs from both wild-type and TMIE mutant mice (Fig. 6*A*). These synaptic events were reversibly blocked by superfusion of 1 μM strychnine, an α9α10 antagonist (*SI Appendix*, Fig. S7*A*). We quantified these synaptic responses at three developmental stages: Neonatal (P2 to P5), second postnatal week (P7 to P12), and third postnatal week (P14 to P18). At early stages, the amplitudes of α9α10-mediated synaptic currents in TMIE mutants were approximately double those in wild-type (Fig. 6 *B* and *C*). In

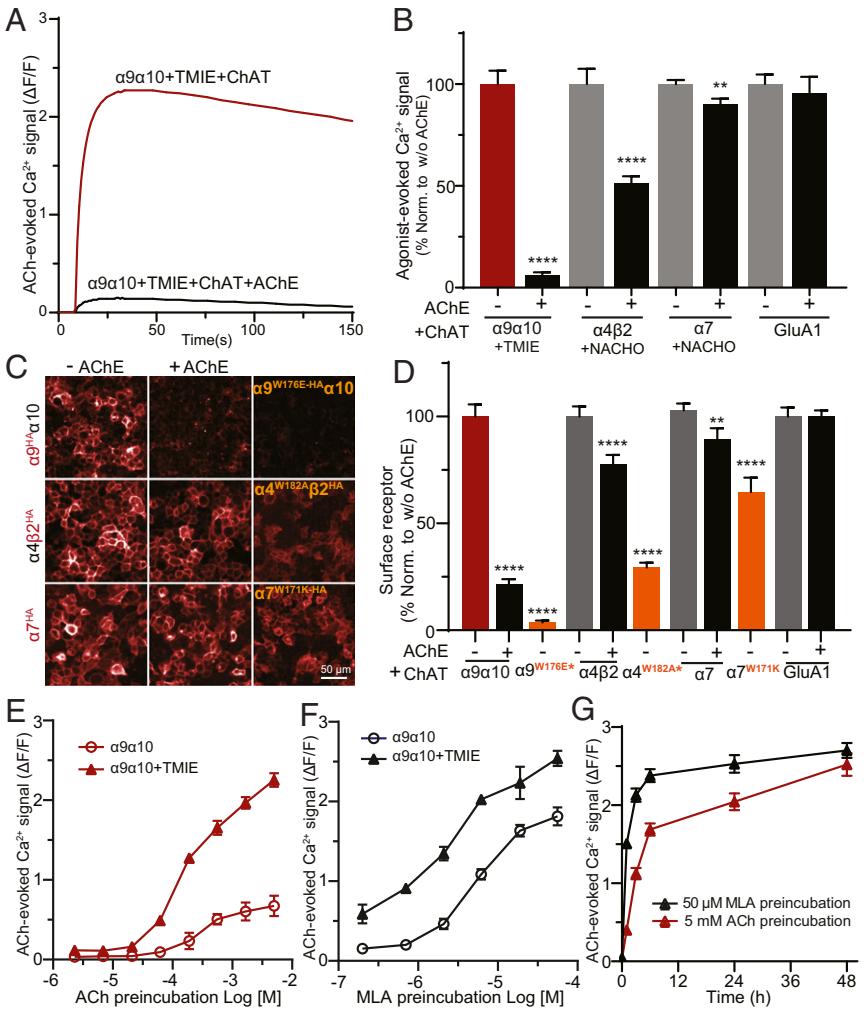

Fig. 3. α9α10 receptor assembly requires ligand binding. (*A*) FLIPR traces from HEK cells transfected with α9α10 + TMIE and ChAT in the presence (black) or absence (red) of AChE. (*B*) Graph quantifies effect of AChE (black) on function of various receptors in the presence of ChAT (mean ± SD, $n = 8$, $^{**}P \leq 0.01$, $^{****}P \leq 0.0001$, for comparison to AChE, one-way ANOVA, Dunnett's test). Agonists used were: ACh (250 μM) for α9α10, α4β2, ACh (250 μM) + PNU120596 (10 μM) for α7; and glutamate (100 μM) + CTZ (100 μM) for GluA1. Whereas AChE fully blocked α9α10 function, AChE only partially blocked α4β2 and α7, whereas AChE had no effect on GluA1. (*C*) Surface HA-labeling of HEK cells transfected as indicated. The W176E and W182A mutations in α9 and α4, respectively, prevent orthosteric ligand-binding. NACHO was included in $\alpha4\beta2^{HA}$ and $\alpha7^{HA}$ transfections; ChAT was present in all transfections. Whereas disruption of ligand-binding abolished α9α10 surface expression, some α4β2 surface expression persisted in the ligand-binding mutant. (*D*) Summary graph of surface labeling of HA-tagged receptors in absence or presence of AChE. Data shown are from a representative experiment (mean ± SD, $n = 5$, $^{**}P \leq 0.01$, $^{****}P \leq 0.0001$, for comparison to AChE, one-way ANOVA, Dunnett's test) that was replicated with similar results. (*E* and *F*) ACh-evoked FLIPR responses from α9α10 ± TMIE transfected cells following 24-h preincubation with ACh (red) or MLA (black) at indicated concentrations (mean ± SD, $n = 3$). (*G*) FLIPR responses from cells cotransfected with α9α10+TMIE and preincubated with ACh or MLA at indicated times. Data shown are from a representative experiment (mean ± SD, $n = 3$) that was replicated with similar results.

addition to amplitude, we observed increased frequency of synaptic events in prehearing TMIE mutant mice, which reflects either increased release probability or that the enhanced amplitude allowed more events to reach the detectable limit. This enhancement of cholinergic responses in TMIE mutants suggested functional redundancy with TMEM132a or TMEM132e, which can also synergize with ChAT for α9α10 channel function and remain expressed in hair cells of TMIE mutant mice (*SI Appendix*, Fig. S7*B*). Furthermore, TMEM132e enhanced α9α10-mediated responses significantly more than did TMIE (*SI Appendix*, Fig. S7*C*).

Beyond the second postnatal week, IHCs lose their medial olivocochlear cholinergic input and their postsynaptic α9α10 receptor function (27). Accordingly, KCl failed to elicit any synaptic responses in wild-type IHCs P14 to P18 (Fig. 6 *B* and *C*). In striking contrast, α9α10-mediated synaptic currents persisted in IHCs of P14 to P18 TMIE mutant mice (Fig. 6 *B* and *C*). To further evaluate this efferent synaptic distinction between wild-type and TMIE mutants, we examined their hair cell innervation using the cholinergic marker vesicular acetylcholine transporter (VAChT). In P7 to P8, VAChT labeling in wild-type and TMIE mutant mice was similar (Fig. 6 *D* and *E*), arguing that altered cholinergic input did not explain enhanced α9α10-mediated transmission at early developmental stages. In P20 TMIE mutants, retention of α9α10-dependent synaptic transmission was associated with IHC innervation by large cholinergic presynaptic terminals (Fig. 6 *D* and *E*). In contrast, P20 wild-type IHCs receive only small cholinergic puncta (Fig. 6 *D* and *E*) (27) typically associated with muscarinic receptors (43).

To assess directly α9α10 function in TMIE mutant mice, we used fluorescent calcium imaging. We incubated acutely-dissected cochlear organs with Fluo-8 AM. ACh application (300 μM) evoked transient strychnine-sensitive calcium responses in IHCs from P11 TMIE mutants whose amplitudes were roughly double those from

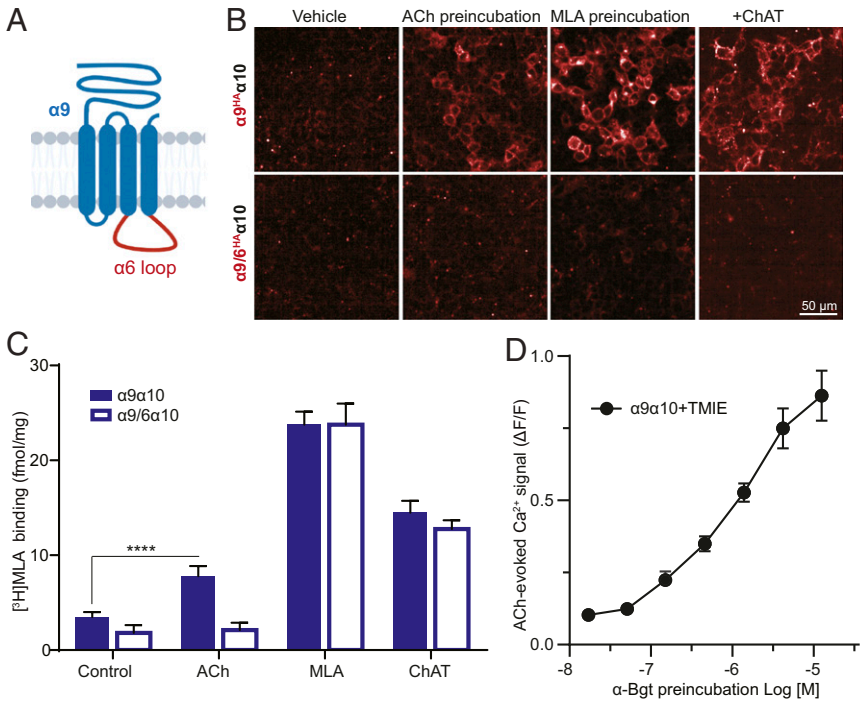

Fig. 4. ACh-mediated α9α10 assembly can occur on the cell surface. (*A*) Schematic α9 (blue) chimera with α6 intracellular loop (red). (*B*) Replacing the α9 cytosolic loop with that from α6 (α9/6^{HA}) blocks receptor surface expression. Surface receptor labeling (red) of intact cells transfected with α9^{HA}α10 or α9/6^{HA}α10 in the absence or presence of ChAT and preincubated where indicated for 24 h with vehicle, ACh (5 mM), or MLA (50 μM). (*C*) Specific [^{3}H]MLA (3 nM) binding to cells transfected with α9^{HA}α10 or α9/6^{HA}α10 in the absence (control) or presence of ChAT and preincubated where indicated for 24 h with ACh (5 mM) or MLA (50 μM). The α6 loop blocked ACh-mediated but not MLA- or ChAT-mediated α9α10 receptor assembly. Data shown are from a representative experiment (mean ± SD, $n = 4$, $^{****}P \leq 0.0001$ for comparison to α9^{HA}α10 control, two-way ANOVA, Sidak's test) that was replicated with similar results. (*D*) ACh-evoked FLIPR responses from cells transfected with α9α10 + TMIE and preincubated for 24 h with α-Bgt at indicated concentrations (mean ± SD, $n = 3$).

wild-type mice (Fig. 6 *F* and *G*). These physiological experiments demonstrate that TMIE mutant mice display enhanced IHC postsynaptic α9α10 activity and that IHC cholinergic innervation and α9α10 function persist beyond the second postnatal week.

Discussion

Genome-Wide cDNA Screening Identifies Factors Necessary for α9α10 Receptor Reconstitution. This study identifies proteins that can reconstitute functional α9α10 receptors in mammalian recombinant cells. These recombinant receptors display the biophysical and pharmacological properties of α9α10 channels recorded in cochlear hair cells. This work shows that subunit assembly and surface expression require cholinergic ligand binding, which is strictly required for biogenesis of α9α10 receptors. Additionally, ion channel activity requires a non-nAChR transmembrane component, including TMIE or TMEM132e, which are coexpressed with α9α10 receptors in hair cells and underlie nonsyndromic clinical deafness (29, 30). We show that mammalian TMIE is a single-pass TM protein, whose actions on α9α10 are evolutionarily conserved at least through Arthropoda. Disruption of TMIE in *Spinner* mice up-regulates postsynaptic nAChR channel activity in cochlear hair cells, which may reflect redundancy with TMEM132e, which we show enhances α9α10 function more robustly than does TMIE. These unexpected results define functions for TMIE and TMEM132e as neurotransmitter receptor accessories and will transform basic research and drug discovery on the hair cell efferent synapse.

Our ability to reconstitute α9α10 relied on a genome-wide expression cloning strategy that we used previously to identify nAChR accessories (44). Such screening identified NACHO, which is essential for assembly of homopentameric α7 (28) and which also promotes function of most heteromeric nAChRs in the brain (45, 46). Cell biological studies demonstrate that NACHO resides in the neuronal endoplasmic reticulum and serves as a client-specific chaperone to mediate nAChR subunit oligomerization and plasma membrane trafficking (28). Whereas α9α10 subunits also fail to properly pentamerize in transfected cells (25), NACHO does not promote function or assembly of α9α10 receptors.

Assembly and Surface Trafficking of α9α10 Strictly Require Ligand Binding. In addition to protein accessories, small molecules can modulate nAChRs assembly. Seminal studies in the 1980s found that smokers have elevated nAChRs levels in the brain, and this receptor up-regulation likely contributes to nicotine addiction (47, 48). Subsequent experiments in animals and neurons found that nicotinic ligands can serve as chemical chaperones to stabilize nAChR pentamers (49). Screening here revealed that ChAT can promote α9α10 function. Whereas ChAT is not present in hair cells, this observation pointed to a critical role for ACh, which is required for α9α10 biogenesis. Indeed, mutating the α9α10 ACh binding site abolishes receptor surface expression. Although α4β2 trafficking can also be enhanced by ChAT, its surface expression is not strictly dependent upon ligand binding. Previous studies showed that ligand binding promotes α4β2 nAChR receptor assembly in the endoplasmic reticulum (50). For α9α10, both intracellular and extracellular cholinergic ligands can enhance surface receptor expression, as this occurs with ACh and even α-Bgt, which do not permeate cell membranes. This robust ligand-mediated functional expression of α9α10 occurs rapidly and likely has physiological consequences.

Developmental studies of IHCs show that postsynaptic α9α10 channels exist only transiently prior to the third week postnatal, and this timing precisely matches the appearance and then retraction of the cholinergic input (26, 27). Fitting with this, several studies suggest that presynaptic innervation may be mechanistically linked to postsynaptic α9α10 functional expression. Importantly,

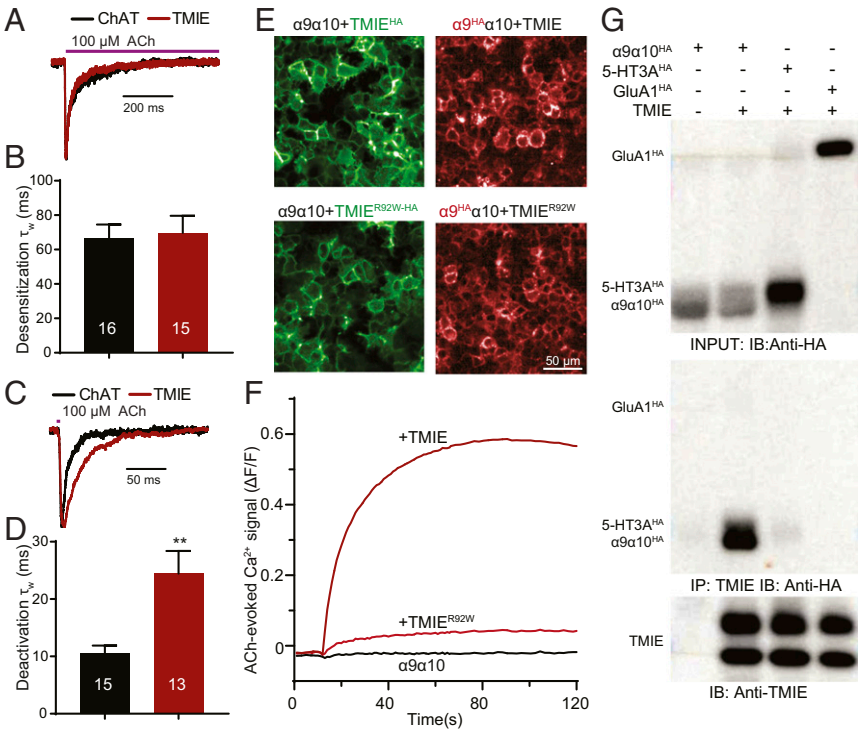

Fig. 5. TMIE regulates α9α10 gating as a receptor auxiliary subunit. (*A–D*) Patch-clamp analysis of cells transfected with α9α10 + ChAT (black) or α9α10 + TMIE (red) and preincubated with 5 mM ACh for 24 h. ACh (100 μM) was applied for 2 s or 2 ms to assess channel desensitization or deactivation, respectively. Representative traces followed by summary graphs are shown (mean ± SEM, *n* as indicated, $^{**}P \leq 0.01$, Student's *t* test). (*E*) Surface labeling for TMIE (green) or α9 (red) in cells cotransfected with ChAT and other plasmids as indicated. TMIE expressed robustly on the cell surface. The TMIE deafness mutation, R92W, did not affect surface expression of $TMIE^{R92W\text{-}HA}$ or that of cotransfected $\alpha9^{HA}\alpha10$. (*F*) FLIPR responses to ACh (250 μM) from cells cotransfected with α9α10 + TMIE or α9α10 + $TMIE^{R92W}$. The R92W mutation disrupted TMIE-mediated reconstitution of α9α10 function. (*G*) Immunoprecipitation (IP) analysis of receptor interactions with TMIE in *Xenopus* oocytes. Solubilized membranes from oocytes coinjected with cRNAs encoding TMIE and $\alpha9\alpha10^{HA}$, $5\text{-}HT3A^{HA}$, or $GluA1^{HA}$ were immunoprecipitated with antibody to TMIE. Input and immunoprecipitation were immunoblotted with anti-HA or anti-TMIE as indicated. Data shown are from an experiment that was replicated with similar results.

transgenic expression of α10 in mature IHCs, which lack cholinergic efferents, does not yield α9α10 channel function despite robust expression of both α9 and α10 (51). In addition, genetic deletion of the SK2 channel leads to olivocochlear fiber degeneration and disrupts hair cell α9α10 function despite preserved expression of α9 and α10 mRNAs (52, 53). Finally, in certain models of age-related hearing loss, mature IHCs regain both cholinergic input and functional α9α10 receptors (54). Strikingly, we also find that third-week postnatal TMIE mutant mice show sustained cholinergic innervation of IHCs and persistent α9α10 activity. The strict requirement of ligand binding for α9α10 surface expression found here may help link innervation with α9α10 functional expression.

α9α10 Channel Activity Requires Auxiliary Subunits. Although ligand binding enables α9α10 surface expression, channel activity additionally requires a TM accessory. Genome-wide screening identified TMIE and TMEM132 family members as functional α9α10 accessories that are also expressed in hair cells. Biochemical and electrophysiological studies of recombinant receptors demonstrate that TMIE functions as an auxiliary subunit that associates stably with α9α10 on the cell surface and modulates channel gating. This is analogous to auxiliary subunit BARP, which modulates mammalian α6β2β3, and MOLO-1 and EAT-18, auxiliary subunits for *Caenorhabditis elegans* nAChRs (46, 55, 56). The TMIE/α9α10 connection is evolutionarily conserved as *Drosophila* TMIE, also a single-pass transmembrane protein whose sequence shares only ~20% identity with human TMIE, enables functional reconstitution of mammalian α9α10.

TMIE was identified independently as the gene recessively mutated in a familial nonsyndromic deafness (29) and in hearing-impaired *Spinner* mice (57). TMIE mRNA encodes a unique protein that lacks homologs and is enriched in neuronal tissues and cochlea (57). TMIE protein localizes both to the stereocilia and to the cell body of cochlear hair cells (31, 33). It is an essential component of the cochlear hair cell MET channel machinery (31), which contains pore-forming proteins, TMC1 and TMC2 (58). In mature cochlea, TMIE mRNA expression is enriched together with α9, α10, and SK2 in OHCs (59, 60), and this expression profile does not match the distribution of MET channel activity. These data and the presence of TMIE protein at hair cell bodies (31) imply multiple roles for TMIE in hair cells.

TMIE mutant mice have enhanced α9α10 function. Prior to postnatal week three, we found that both synaptic and ACh-evoked α9α10 function in IHCs of TMIE mutants are increased ~100% and that channel activity persists through developmental stages that typically lose IHC α9α10 activity and medial olivocochlear innervation (2, 3). In contrast, IHC α9α10 currents are normal at postnatal day 8 in deaf $Ca_v1.3$ knockout mice (61), suggesting that increased α9α10 activity in TMIE mutants is specific and not an obligate consequence of deafness. The functional postsynaptic enhancement of α9α10 in TMIE mutants may reflect receptor association with TMEM132a or TMEM132e proteins, which are expressed in cochlear hair cells and in which TMEM132e has greater activity on α9α10 than does TMIE. TMEM132 family members are plasma membrane cell-adhesion proteins with poorly-defined molecular functions (62). Importantly, recessive TMEM132e mutation causes nonsyndromic hearing loss, and TMEM132e is required

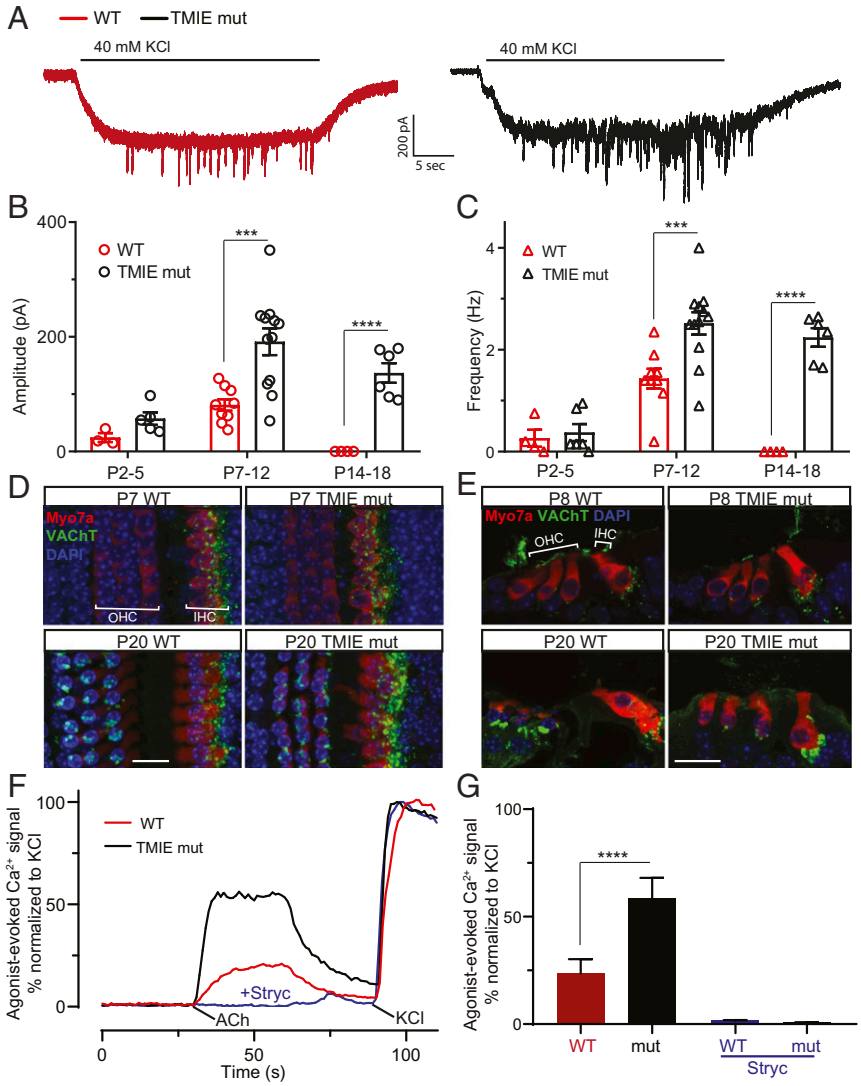

Fig. 6. Up-regulation of α9α10 function in *Spinner* TMIE mutant mice. (*A*) Electrophysiological recordings of synaptic activity from IHCs of P8 wild-type (WT; red) or P9 TMIE mutant (TMIE mut; black) mice. As indicated, 40 mM KCl induced a sustained inward current with overlaid synaptic events at a holding potential of −80 mV. (*B* and *C*) Quantification of average amplitude and frequency of IHC synaptic current at P2 to P5, P7 to P12, and P14 to P18 time points in wild-type or TMIE mutant mice. Individual data points indicate average values of a single cell (mean ± SEM, $n = 4, 6, 9, 12, 4, 6$ from left to right in amplitude and frequency analysis. $^{***}P \leq 0.001$, $^{****}P \leq 0.0001$, two-way ANOVA, Sidak's test). (*D* and *E*) Immunofluorescence on whole-mount (*D*) and transverse (*E*) sections of mouse organ of Corti show that in P7-8 mice, VAChT labeling of innervation beneath IHCs was similar in wild-type and TMIE mutants. In P20 mice, wild-type displayed only small VAChT positive puncta at the base of IHCs, whereas TMIE mutants had large cholinergic terminals on IHCs. Myo7a labels the three rows of OHCs and IHCs. (Scale bar, 10 μm for *D* and 20 μm for *E*.) (*F*) Fluorescent calcium imaging of IHCs from P11 wild-type (red) or TMIE mutant (black) mice. As indicted, 300 μM ACh was applied followed by 40 mM KCl. Pretreatment and coapplication with 10 μM strychnine (blue) abolished ACh-evoked fluorescence change in both the wild-type and TMIE mutant. (*G*) Quantification graph of ACh-evoked peak response. Data shown are from a representative experiment (mean ± SD, $n = 7$, $^{****}P \leq 0.0001$ for comparison to wild-type, one-way ANOVA, Dunnett's test).

for normal function of the MET channel (30). However, TMEM132e protein does not localize to the IHC stereocilia, where the MET channel largely occurs (31), but is enriched at the base of mature hair cells (30) where α9α10 receptors function. Whereas effects on α9α10 cannot explain the profound hearing impairment associated with mutation of either TMIE or TMEM132e, these proteins clearly regulate multiple ion channels in cochlear hair cells. Future studies of mice with compound knockouts of TMIE, TMEM132a, and TMEM132e are needed to define the essential role and redundancies for these proteins on α9α10 function.

Our screening also identified that TMEM100 and TNFRSF10a, but no other human cDNAs, can synergize with ChAT to enable functional α9α10 receptors. TMEM100 is a small two-pass TM protein that is expressed in dorsal root ganglion neurons, where it regulates a TRPA1–TRPV1 complex and modulates persistent pain (63). Pharmacological antagonism or genetic disruption of α9α10 receptors blunt neuropathic pain (64), and both α9 and α10 mRNAs are expressed in human dorsal root ganglion neurons (65), suggesting a possible role for TMEM100 in regulating α9α10 receptors in sensory neurons. TNFRSF10a is a TRAIL receptor enriched in leukocytes (66). Interestingly, these cells also express α9α10 receptors, which have been linked to nicotine-mediated antiinflammatory responses (67). Whereas TMIE, TMEM132, TMEM100, and TNFRSF10a lack sequence homology, all are cell surface, integral membrane proteins. By analogy, a distinct collection of dissimilar plasma membrane proteins function as auxiliary subunits of AMPA-type glutamate receptors (68).

Physiological and Translational Implications. Functional reconstitution of α9α10 receptors in mammalian cells has important biochemical and biomedical implications. From a basic science perspective, α9α10 receptors have intriguing pharmacological and electrophysiological properties that show peculiar divergence across species (69). Our reconstruction of α9α10 now enables robust biophysical studies that have not previously been feasible. From a translational science perspective, hearing loss is globally the fourth leading cause of years lived with disability, and its prevalence is growing with the aging population (70). The medial olivocochlear nucleus provides a negative feedback system that inhibits amplification of sounds by OHCs. Genetic enhancement of α9α10 receptors in this pathway can protect and even repair the inner ear sensory system from acoustic trauma damage (24, 71). In addition, the abnormal reemergence of cholinergic efferents on IHCs associated with age-related hearing loss may participate in the pathophysiology of tinnitus (54). Whereas α9α10 provides a compelling target for these major unmet medical needs, efficient drug development has not previously been feasible. Our research enables high-throughput screening and identification of pharmacological agents to modulate α9α10 receptor function for auditory and vestibular disorders.

Methods

Genes and Materials. The genes studied here were: Human *CHRNA9* (NM_017581); *CHRNA10* (NM_020402); *TMIE* (NM_147196); *CHAT* (NM_020984); *ACHE* (NM_015831); *CHRNA7* (NM_000746); *TMEM35* (NM_021637); *CHRNA4* (NM_000744); *CHRNB2* (NM_000748); *GRIA1* (NM_001114183); mouse *HTR3A* (NM_013561); rat *CHRNA9* (NM_022930); rat *CHRNA10* (NM_022639); *Drosophila* TMIE (NM_001259175). Modified DNA constructs used the follow oligonucleotides: C-terminal HA-tagged α9 (NFVEAVSKDFAPSGAYPYDVPDYA), N- HA–tagged TMIE(G6:G8); extracellular HA-tagged TMIE (T34:P36), C- HA–tagged TMIE (P110: P111), the SP of TMIE (M1-A26) was replaced with GluA1 signal peptide (M1-G18). Other HA-tagged constructs were described previously (28, 45). Amino acids for chimeric constructs were: Chimeric α7 (M1-P328:S458-A502) with α6 loop (R339-E453), and chimeric α9 (M1-P334:S446-D479) with α6 loop (R339-E453). HEK293T/17 cell lines were purchased from ATCC. The brain-enriched cDNA library was constructed by selecting the 3025 human cDNA clones with the highest ratio of mean mRNA expression in CNS (hippocampus, striatum, cerebral cortex, and thalamus) versus peripheral tissues (stomach, liver, kidney, heart, skeletal muscle, and spleen). Other cDNA libraries were purchased from Origene (28) and The Broad Institute (36). Anti-HA antibody conjugated with Dylight 650 and α-Bgt conjugated with Alexa Fluor 647 were from Thermo scientific. Rabbit anti-TMIE (PA5-58330) antibody and mouse anti-HA antibody (26183) were from Thermo Scientific. [^{3}H]MLA (ART0882A) was purchase from American Radiolabeled Chemicals. *Xenopus* oocytes were purchased from Ecocyte. All chemicals and pharmacological compounds were from Sigma and Tocris. The TMIE mutant mice (*Tmie^{sr-2J}*, Cat #008834) was purchased from the Jackson Laboratory. This mutant line carries a G-to-A transition in the critical G nucleotide of the 3′ splice acceptor site adjacent to exon 5, which disrupts TMIE protein function.

FLIPR Assay for Ca^{2+} in HEK Cells. High-throughput FLIPR assays were performed using HEK cells in 384-well plates. Briefly, cells were seeded at 1×10^4 cells per well and transfected 4 h after seeding with Fugene 6. After overnight incubation at 37 °C, cells were transferred to 30 °C for another 24 h. Then, cells were washed three times with assay buffer (137 mM NaCl, 4 mM KCl, 2 mM $CaCl_2$, 1 mM $MgCl_2$, 5 mM glucose, 10 mM Hepes pH 7.4) and loaded with Calcium5 dye (Molecular Devices) containing 1.25 mM probenecid for 1 h at room temperature. After three washes, plates were placed on the FLIPR stage. After establishing a baseline, 250 μM ACh was applied for a 2-min recording. Scopolamine (50 nM) was used to inhibit endogenous muscarinic receptor-mediated responses.

Immunofluorescent Staining and Opera Imaging. HEK cells were cultured and transfected in 384-well plates from PerkinElmer. Cells were cotransfected with GFP for reference. For surface staining, cells were incubated with Dylight 650 anti-HA antibody at 1:1,000 dilution in culture medium for 30 min at 30 °C. Cells were washed and then fixed with 4% paraformaldehyde for 45 min. Cells were washed three times and incubated with NucBlue reagent (ThermoFisher Scientific) for nuclear staining. Images were captured using the Opera Phenix imaging system. For total staining, prior to antibody incubation, HEK cells were fixed and permeabilized with 0.3% Triton X-100 for 30 min. Fluorescence measurements are quantified and analyzed using the Columbus Image Data Storage and Analysis System. Cells transfected with GFP alone were used to calculate nonspecific antibody binding.

For cochlear staining, mice were perfused transcardially with 4% paraformaldehyde in PBS. Cochlea were dissected and left in fixative overnight at 4 °C. P20 cochlea were decalcified using Bone Decalcification Buffer (Advanced Cell Diagnostics). Organ of Corti were dissected and membranes removed for whole-mount immunostaining, or sucrose protected and mounted in OCT embedding medium for slicing.

For whole-mount immunostaining, organs were blocked and permeabilized in PBS containing 1% Triton X-100, 5% donkey serum, and 5% BSA. Primary antibodies (guinea pig anti-VAChT, Synaptic Systems, 1:200; rabbit anti-Myosin VIIA, *Proteus* Biosciences, 1:1,000) were incubated in PBS containing 2% BSA and 0.1% Triton X-100 at 37 °C in a humidified chamber for 24 h, and another 24 h at room temperature. Alexa Fluor-conjugated secondary antibodies were diluted 1:250 in PBS containing 1% BSA and 0.1% Triton X-100 and incubated for 3 h at 37 °C. Organs were mounted using Vectashield HardSet mounting medium with DAPI. Images were collected using a 40× oil-immersion objective on the Carl Zeiss LSM 700 confocal microscope and Zen software.

For transverse sections, organs of Corti were cut into 12-μm cryostat sections. Slices were blocked for 1 h at room temperature with 10% BSA in 0.1% Triton-X100. Primary antibodies were incubated overnight in 0.1% Triton-X100 and 1% BSA at 4 °C. Secondary antibodies were incubated for 2 h at room temperature.

Electrophysiology. For transfected HEK293T cell recording, cells were transfected using Fugene 6. At 48 to 72 h posttransfection, cells were transferred to the recording chamber submerged in solution composed of: 137 mM NaCl, 10 mM Hepes, 5 mM glucose, 4 mM KCl, 2 mM $CaCl_2$, 1 mM $MgCl_2$, pH 7.4, 300 mOsm. Transfected cells were identified with GFP. Whole-cell recordings were acquired using intracellular solution composed of: 140 mM potassium gluconate, 10 mM Hepes, 4 mM Mg-ATP, 0.4 mM Na-GTP, and 0.6 mM EGTA, pH 7.3, 290 mOsm. Fast perfusion of compounds was achieved with the Perfusion Fast-Step system (Warner Instruments). To study desensitization and deactivation kinetics, ultrafast perfusion of compounds used a piezo-driven perfusion system and theta glass (Siskiyou). All recordings were done at room temperature, and the membrane potentials were held at –60 mV. Recordings were performed using AxoPatch 200B amplifier (Molecular Devices), signals were filtered at 2 kHz, and digitized at 10 kHz. Data acquisition and on-line analysis were done using pClamp 9 (Axon Instruments). All whole-cell recordings from GFP$^+$ cells were included in the analysis for statistical comparisons.

For the IHC recordings, the organ of Corti was dissected from mice at ages specified. The apical turns of the organ of Corti were isolated and pinned to a glass coverslip, visualized with differential interference contrast, and used for recordings within 2 h of dissection. Recordings were performed in HyClone Hepes buffer extracellular solution containing: 149 mM NaCl, 4 mM KCl, 10 mM Hepes, 5 mM glucose, 1.3 mM $CaCl_2$, 0.9 mM $MgCl_2$, 0.7 mM NaH_2PO_4, pH 7.4 under constant perfusion at room temperature. IHCs were visualized with a water immersive 40× objective (Olympus). In <P12 slices, Kollikers organ was cleared via negative pressure through a broken-tip recording pipette to expose basal ends of IHCs.

Pipettes for recording were pulled from borosilicate glass (World Precision Instruments) and had final resistances of 4 to 10 MΩ. Pipette internal solution comprised: 140 mM K-gluconate, 10 mM Hepes, 4 mM Mg-ATP, 0.4 mM Na-GTP, and 0.6 mM EGTA, pH 7.3, 290 mOsm. For recordings, cells were held at –80 mV and stimulated with local application of 40 mM KCl via a perfusion pencil to depolarize efferent inputs and evoke synaptic events. The data were recorded using a Multiclamp 700B amplifier. Resistance was monitored before and after recordings and cells were discarded if access resistance exceeded 20 MΩ. Quantification of synaptic events were performed in Clampfit (Molecular Devices) or OriginPro 2020 (OriginLab).

[^{3}H]MLA Binding. Transfected HEK 293T cells were harvested and resuspended in 50 mM ice-cold Tris·HCl buffer (pH 7.4). Cells were homogenized for 30 s at high speed using an Ika T-25 Ultra-Turrax. Cell lysates were centrifugated at 1,000 × *g* for 10 min at 4 °C to remove cell debris. Protein concentrations were determined with BCA assays using a commercial reagent (Thermo Scientific).

[^{3}H]MLA binding assays were performed in 96-well plates. For each well, cell lysates (~0.2 mg/mL) were incubated with 10 or 3 nM [^{3}H]MLA in a total volume of 100 μL. Nonspecific binding was determined by coincubation with 10 μM unlabeled MLA. Binding assays were terminated by filtration through PEI (0.3%) coated GF/B filters and washed three times with 500 mL ice-cold

assay buffer per plate. Filter plates were desiccated at 65 °C for 30 min and incubated with 70 μL MicroScint-0. Bound [^{3}H]MLA was quantified using TopCount.

Immunoprecipitation from *Xenopus* Oocytes. *Xenopus* oocytes from Ecocyte were cultured in Modified Barth's Saline (F-04-B) from Sigma. cRNAs were synthesized using mMESSAGE mMACHINE T7 ULTRA Transcription Kit (AM1345). The optimized cRNAs amounts injected per oocyte were: 4 ng of nAChR α9, 2 ng of nAChR $\alpha10^{HA}$, 10 ng of TMIE, 3 ng of $GluA1^{HA}$, or 1 ng of $5\text{-}HT3A^{HA}$. Injected oocytes were incubated at 18 °C for 3 d. Oocytes were harvested and lysed in buffer containing 50 mM Hepes pH7.4, 100 mM NaCl, 1 mM EDTA, and protease inhibitors. Cell debris was removed by centrifugation at 1,000 × g for 15 min. Cell lysates were solubilized with 1% DDM and incubated for 2 h on ice. Non-solubilized material was removed by centrifugation at 20,000 × *g* for 30 min. Solubilized fractions were incubated with anti-TMIE antibody overnight at 4 °C. Protein G magnetic beads were used to antibodies and associated proteins. After three washes, proteins were eluted by incubating with 1× SDS sample buffer at 50 °C for 15 min and then were processed for immunoblotting.

Cochlear Hair Cell Calcium Imaging. The organ of Corti of P11 C57BL/6 and TMIE mutant mouse pups were prepared as described in ref. 72. Briefly, the organ was dissected, and the tectorial membrane removed in a solution containing: 143 mM NaCl, 5.8 mM KCl, 1.3 mM $CaCl_2$, 0.8 mM $MgCl_2$, 5.6 mM glucose, 10 mM Hepes, and titrated NaH_2PO_4, 305 mOsm/L, pH 7.35. The apical turn of the organ was mounted to one end in a 35-mm glass dish with a 0.1-mm minutien pin. The immobilized tissue was incubated with 10 μM Fluo-8 AM (AAT Bioquest) for 40 to 60 min. After four washes with perilymph solution, the organ of Corti was subjected to imaging analysis using a microscopy LSM 700. The sequential application of 300 μM ACh and 40 mM KCl evoked a calcium signal, which was recorded using Zeiss software and analyzed using Imaris imaging software (Bitplane). Strychnine (10 μM) pre-incubation was used to block the ACh-evoked calcium signal. A final KCl-evoked signal was evoked for normalization. The average fluorescence intensity of each cell was measured over the course of each experiment and plotted using GraphPad Prism.

RNAscope In Situ Hybridization. The RNAscope protocol was performed as described in ref. 73. Briefly, P8 to P9 mice were intracardially perfused with 4% PFA, and the organ of Corti quickly dissected and fixed for 1 h. Slices were dehydrated in a series of graded methanol steps and treated with Protease III solution (ACD Biosciences) for 12 min at room temperature. RNA Probes were hybridized (three probes per sample) overnight at 40 °C in a humidified chamber. Probe amplification steps (AMP1 to AMP4) were performed according to the ACD manual with a series of 3 × 0.2× SSC 15-min wash steps in between amplifications. Tissues were incubated with DAPI and mounted with ProLong Gold Antifade Mountant (ThermoFisher). Images were taken using a Zeiss confocal microscope with an oil immersion 63× objective.

Statistics. Data represented as mean ± SEM are the result of at least three independent experiments. Data shown as mean ± SD are from a representative experiment that was replicated with similar results. Analyses involving two datasets were performed with an unpaired *t*-test. Analyses involving three or more datasets were performed with a one-way ANOVA using GraphPad Prism software. Significance was set as $P < 0.05$.

Materials and Protocols. All materials and protocols in this manuscript are indicated in *Methods*. All animal work was overseen by an Association for Assessment and Accreditation of Laboratory Animal Care-accredited institutional review board.

Data Availability. All of the data are included in the main text and *SI Appendix*.

ACKNOWLEDGMENTS. The authors thank Drs. Marcelo Moglie, Juan Goutman, Carolina Wedemeyer, and the rest of the laboratory of Dr. Ana Belén Elgoyhen (University of Buenos Aires) for teaching us the methodology for electrophysiological recordings of inner hair cells; and Dr. Xiang Yao (Janssen) for bioinformatic analyses.

1. R. Klinke, N. Galley, Efferent innervation of vestibular and auditory receptors. *Physiol. Rev.* **54**, 316–357 (1974).
2. P. A. Fuchs, A. M. Lauer, Efferent inhibition of the cochlea. *Cold Spring Harb. Perspect. Med.* **9**, a033530 (2019).
3. A. B. Elgoyhen, E. Katz, The efferent medial olivocochlear-hair cell synapse. *J. Physiol. Paris* **106**, 47–56 (2012).
4. C. Blanchet, C. Eróstegui, M. Sugasawa, D. Dulon, Acetylcholine-induced potassium current of guinea pig outer hair cells: Its dependence on a calcium influx through nicotinic-like receptors. *J. Neurosci.* **16**, 2574–2584 (1996).
5. P. Dallos *et al.*, Acetylcholine, outer hair cell electromotility, and the cochlear amplifier. *J. Neurosci.* **17**, 2212–2226 (1997).
6. A. B. Elgoyhen, E. Katz, P. A. Fuchs, The nicotinic receptor of cochlear hair cells: A possible pharmacotherapeutic target? *Biochem. Pharmacol.* **78**, 712–719 (2009).
7. M. Zouridakis *et al.*, Crystal structure of the monomeric extracellular domain of α9 nicotinic receptor subunit in complex with α-conotoxin RgIA: Molecular dynamics insights into RgIA binding to α9α10 nicotinic receptors. *Front. Pharmacol.* **10**, 474 (2019).
8. L. W. Role, D. K. Berg, Nicotinic receptors in the development and modulation of CNS synapses. *Neuron* **16**, 1077–1085 (1996).
9. C. Gotti, F. Clementi, Neuronal nicotinic receptors: From structure to pathology. *Prog. Neurobiol.* **74**, 363–396 (2004).
10. J. Lindstrom, Nicotinic acetylcholine receptors in health and disease. *Mol. Neurobiol.* **15**, 193–222 (1997).
11. R. C. Hogg, M. Raggenbass, D. Bertrand, Nicotinic acetylcholine receptors: From structure to brain function. *Rev. Physiol. Biochem. Pharmacol.* **147**, 1–46 (2003).
12. N. Le Novère, P. J. Corringer, J. P. Changeux, The diversity of subunit composition in nAChRs: Evolutionary origins, physiologic and pharmacologic consequences. *J. Neurobiol.* **53**, 447–456 (2002).
13. M. R. Picciotto, Nicotine as a modulator of behavior: Beyond the inverted U. *Trends Pharmacol. Sci.* **24**, 493–499 (2003).
14. R. L. Papke, Merging old and new perspectives on nicotinic acetylcholine receptors. *Biochem. Pharmacol.* **89**, 1–11 (2014).
15. A. B. Elgoyhen, D. S. Johnson, J. Boulter, D. E. Vetter, S. Heinemann, Alpha 9: An acetylcholine receptor with novel pharmacological properties expressed in rat cochlear hair cells. *Cell* **79**, 705–715 (1994).
16. A. B. Elgoyhen *et al.*, alpha10: A determinant of nicotinic cholinergic receptor function in mammalian vestibular and cochlear mechanosensory hair cells. *Proc. Natl. Acad. Sci. U.S.A.* **98**, 3501–3506 (2001).
17. M. Lipovsek *et al.*, Tracking the molecular evolution of calcium permeability in a nicotinic acetylcholine receptor. *Mol. Biol. Evol.* **31**, 3250–3265 (2014).
18. D. E. Vetter *et al.*, Role of alpha9 nicotinic ACh receptor subunits in the development and function of cochlear efferent innervation. *Neuron* **23**, 93–103 (1999).
19. D. E. Vetter *et al.*, The alpha10 nicotinic acetylcholine receptor subunit is required for normal synaptic function and integrity of the olivocochlear system. *Proc. Natl. Acad. Sci. U.S.A.* **104**, 20594–20599 (2007).
20. A. Clause, A. M. Lauer, K. Kandler, Mice lacking the Alpha9 subunit of the nicotinic acetylcholine receptor exhibit deficits in frequency difference limens and sound localization. *Front. Cell. Neurosci.* **11**, 167 (2017).
21. G. Terreros, P. Jorratt, C. Aedo, A. B. Elgoyhen, P. H. Delano, Selective attention to visual stimuli using auditory distractors is altered in alpha-9 nicotinic receptor subunit knock-out mice. *J. Neurosci.* **36**, 7198–7209 (2016).
22. V. Murthy, J. Taranda, A. B. Elgoyhen, D. E. Vetter, Activity of nAChRs containing alpha9 subunits modulates synapse stabilization via bidirectional signaling programs. *Dev. Neurobiol.* **69**, 931–949 (2009).
23. A. Clause *et al.*, The precise temporal pattern of prehearing spontaneous activity is necessary for tonotopic map refinement. *Neuron* **82**, 822–835 (2014).
24. L. E. Boero *et al.*, Enhancement of the medial olivocochlear system prevents hidden hearing loss. *J. Neurosci.* **38**, 7440–7451 (2018).
25. E. R. Baker, R. Zwart, E. Sher, N. S. Millar, Pharmacological properties of alpha 9 alpha 10 nicotinic acetylcholine receptors revealed by heterologous expression of subunit chimeras. *Mol. Pharmacol.* **65**, 453–460 (2004).
26. B. J. Morley, D. D. Simmons, Developmental mRNA expression of the alpha10 nicotinic acetylcholine receptor subunit in the rat cochlea. *Brain Res. Dev. Brain Res.* **139**, 87–96 (2002).
27. E. Katz *et al.*, Developmental regulation of nicotinic synapses on cochlear inner hair cells. *J. Neurosci.* **24**, 7814–7820 (2004).
28. S. Gu *et al.*, Brain α7 nicotinic acetylcholine receptor assembly requires NACHO. *Neuron* **89**, 948–955 (2016).
29. S. Naz *et al.*, Mutations in a novel gene, TMIE, are associated with hearing loss linked to the DFNB6 locus. *Am. J. Hum. Genet.* **71**, 632–636 (2002).
30. J. Li *et al.*, Whole-exome sequencing identifies a variant in TMEM132E causing autosomal-recessive nonsyndromic hearing loss DFNB99. *Hum. Mutat.* **36**, 98–105 (2015).
31. C. L. Cunningham *et al.*, TMIE defines pore and gating properties of the mechanotransduction channel of mammalian cochlear hair cells. *Neuron* **107**, 126–143.e8 (2020).
32. D. I. Scheffer, J. Shen, D. P. Corey, Z. Y. Chen, Gene expression by mouse inner ear hair cells during development. *J. Neurosci.* **35**, 6366–6380 (2015).
33. M. J. Shin *et al.*, Spatiotemporal expression of tmie in the inner ear of rats during postnatal development. *Comp. Med.* **60**, 288–294 (2010).
34. M. Eybalin, R. Pujol, Choline acetyltransferase (ChAT) immunoelectron microscopy distinguishes at least three types of efferent synapses in the organ of Corti. *Exp. Brain Res.* **65**, 261–270 (1987).
35. B. Zhao *et al.*, TMIE is an essential component of the mechanotransduction machinery of cochlear hair cells. *Neuron* **84**, 954–967 (2014).

36. X. Yang *et al*., A public genome-scale lentiviral expression library of human ORFs. *Nat. Methods* **8**, 659–661 (2011).
37. A. Kuryatov, J. Luo, J. Cooper, J. Lindstrom, Nicotine acts as a pharmacological chaperone to up-regulate human alpha4beta2 acetylcholine receptors. *Mol. Pharmacol.* **68**, 1839–1851 (2005).
38. A. V. Shivange *et al*., Determining the pharmacokinetics of nicotinic drugs in the endoplasmic reticulum using biosensors. *J. Gen. Physiol.* **151**, 738–757 (2019).
39. A. B. Jensen, K. Hoestgaard-Jensen, A. A. Jensen, Elucidation of molecular impediments in the α6 subunit for in vitro expression of functional α6β4* nicotinic acetylcholine receptors. *J. Biol. Chem.* **288**, 33708–33721 (2013).
40. P. Whiteaker, C. G. Sharples, S. Wonnacott, Agonist-induced up-regulation of alpha4beta2 nicotinic acetylcholine receptors in M10 cells: Pharmacological and spatial definition. *Mol. Pharmacol.* **53**, 950–962 (1998).
41. T. Yamasaki, E. Hoyos-Ramirez, J. S. Martenson, M. Morimoto-Tomita, S. Tomita, GARLH family proteins stabilize GABAA receptors at synapses. *Neuron* **93**, 1138–1152.e6 (2017).
42. E. Glowatzki, P. A. Fuchs, Cholinergic synaptic inhibition of inner hair cells in the neonatal mammalian cochlea. *Science* **288**, 2366–2368 (2000).
43. S. F. Maison *et al*., Muscarinic signaling in the cochlea: Presynaptic and postsynaptic effects on efferent feedback and afferent excitability. *J. Neurosci.* **30**, 6751–6762 (2010).
44. M. P. Maher, J. A. Matta, S. Gu, M. Seierstad, D. S. Bredt, Getting a handle on neuropharmacology by targeting receptor-associated proteins. *Neuron* **96**, 989–1001 (2017).
45. J. A. Matta *et al*., NACHO mediates nicotinic acetylcholine receptor function throughout the brain. *Cell Rep.* **19**, 688–696 (2017).
46. S. Gu *et al*., alpha6-containing nicotinic acetylcholine receptor reconstitution involves mechanistically distinct accessory components. *Cell Rep.* **26**, 866–874.e3 (2019).
47. R. D. Schwartz, K. J. Kellar, Nicotinic cholinergic receptor binding sites in the brain: Regulation in vivo. *Science* **220**, 214–216 (1983).
48. H. A. Lester *et al*., Nicotine is a selective pharmacological chaperone of acetylcholine receptor number and stoichiometry. Implications for drug discovery. *AAPS J.* **11**, 167–177 (2009).
49. S. Wonnacott, The paradox of nicotinic acetylcholine receptor upregulation by nicotine. *Trends Pharmacol. Sci.* **11**, 216–219 (1990).
50. J. Sallette *et al*., Nicotine upregulates its own receptors through enhanced intracellular maturation. *Neuron* **46**, 595–607 (2005).
51. J. Taranda *et al*., Constitutive expression of the alpha10 nicotinic acetylcholine receptor subunit fails to maintain cholinergic responses in inner hair cells after the onset of hearing. *J. Assoc. Res. Otolaryngol.* **10**, 397–406 (2009).
52. J. H. Kong, J. P. Adelman, P. A. Fuchs, Expression of the SK2 calcium-activated potassium channel is required for cholinergic function in mouse cochlear hair cells. *J. Physiol.* **586**, 5471–5485 (2008).
53. V. Murthy *et al*., SK2 channels are required for function and long-term survival of efferent synapses on mammalian outer hair cells. *Mol. Cell. Neurosci.* **40**, 39–49 (2009).
54. S. P. Zachary, P. A. Fuchs, Re-emergent inhibition of cochlear inner hair cells in a mouse model of hearing loss. *J. Neurosci.* **35**, 9701–9706 (2015).
55. T. Boulin *et al*., Positive modulation of a Cys-loop acetylcholine receptor by an auxiliary transmembrane subunit. *Nat. Neurosci.* **15**, 1374–1381 (2012).
56. S. Choudhary *et al*., EAT-18 is an essential auxiliary protein interacting with the non-alpha nAChR subunit EAT-2 to form a functional receptor. *PLoS Pathog.* **16**, e1008396 (2020).
57. K. L. Mitchem *et al*., Mutation of the novel gene Tmie results in sensory cell defects in the inner ear of spinner, a mouse model of human hearing loss DFNB6. *Hum. Mol. Genet.* **11**, 1887–1898 (2002).
58. Y. Jia *et al*., TMC1 and TMC2 proteins are pore-forming subunits of mechanosensitive ion channels. *Neuron* **105**, 310–321.e3 (2020).
59. H. Liu *et al*., Characterization of transcriptomes of cochlear inner and outer hair cells. *J. Neurosci.* **34**, 11085–11095 (2014).
60. Y. Li *et al*., Transcriptomes of cochlear inner and outer hair cells from adult mice. *Sci. Data* **5**, 180199 (2018).
61. A. Brandt, J. Striessnig, T. Moser, CaV1.3 channels are essential for development and presynaptic activity of cochlear inner hair cells. *J. Neurosci.* **23**, 10832–10840 (2003).
62. L. Sanchez-Pulido, C. P. Ponting, TMEM132: An ancient architecture of cohesin and immunoglobulin domains define a new family of neural adhesion molecules. *Bioinformatics* **34**, 721–724 (2018).
63. H. J. Weng *et al*., Tmem100 is a regulator of TRPA1-TRPV1 complex and contributes to persistent pain. *Neuron* **85**, 833–846 (2015).
64. H. K. Romero *et al*., Inhibition of α9α10 nicotinic acetylcholine receptors prevents chemotherapy-induced neuropathic pain. *Proc. Natl. Acad. Sci. U.S.A.* **114**, E1825–E1832 (2017).
65. P. Ray *et al*., Comparative transcriptome profiling of the human and mouse dorsal root ganglia: An RNA-seq-based resource for pain and sensory neuroscience research. *Pain* **159**, 1325–1345 (2018).
66. A. Ashkenazi, V. M. Dixit, Death receptors: Signaling and modulation. *Science* **281**, 1305–1308 (1998).
67. Q. Liu *et al*., Attenuation in nicotinic acetylcholine receptor α9 and α10 subunit double knock-out mice of experimental autoimmune encephalomyelitis. *Biomolecules* **9**, 827 (2019).
68. J. Schwenk *et al*., High-resolution proteomics unravel architecture and molecular diversity of native AMPA receptor complexes. *Neuron* **74**, 621–633 (2012).
69. I. Marcovich *et al*., Distinct evolutionary trajectories of neuronal and hair cell nicotinic acetylcholine receptors. *Mol. Biol. Evol.* **37**, 1070–1089 (2020).
70. B. S. Wilson, D. L. Tucci, G. M. O'Donoghue, M. H. Merson, H. Frankish, A Lancet Commission to address the global burden of hearing loss. *Lancet* **393**, 2106–2108 (2019).
71. L. E. Boero *et al*., Preventing presbycusis in mice with enhanced medial olivocochlear feedback. *Proc. Nat. Acad. Sci. U.S.A.* **117**, 11811–11819 (2020).
72. T. Eckrich, K. Blum, I. Milenkovic, J. Engel, Fast Ca^{2+} transients of inner hair cells arise coupled and uncoupled to Ca^{2+} waves of inner supporting cells in the developing mouse cochlea. *Front. Mol. Neurosci.* **11**, 264 (2018).
73. J. Kersigo *et al*., A RNAscope whole mount approach that can be combined with immunofluorescence to quantify differential distribution of mRNA. *Cell Tissue Res.* **374**, 251–262 (2018).